

## Article

# Supported Imidazolium-Based Ionic Liquids on a Polysulfone Matrix for Enhanced CO<sub>2</sub> Capture

David Domingo Huguet <sup>1,2</sup> , Aitor Gual <sup>1</sup> , Ricard Garcia-Valls <sup>1,3</sup> and Adrianna Nogalska <sup>1,\*</sup> 

<sup>1</sup> Eurecat, Centre Tecnològic de Catalunya, Unitat de Tecnologia Química, C/Marcel·lí Domingo, 2, 43007 Tarragona, Spain

<sup>2</sup> Faculty of Chemistry, Universitat Rovira I Virgili, C/Marcel·lí Domingo, 1, 43007 Tarragona, Spain

<sup>3</sup> Department of Chemical Engineering, Universitat Rovira I Virgili, Av. Països Catalans, 26, 43007 Tarragona, Spain

\* Correspondence: adrianna.nogalska@eurecat.org; Tel.: +34-977-297-089

**Abstract:** The present work demonstrates the potential for improved CO<sub>2</sub> capture capabilities of ionic liquids (ILs) by supporting them on a polysulfone polymeric matrix. CO<sub>2</sub> is one of the main gases responsible for the greenhouse effect and is a focus of The European Commission, which committed to diminishing its emission to 55% by 2023. Various ILs based on combinations of 1-butyl-3-methyl-imidazolium cations and different anions (BMI-X) were synthesized and supported on a polysulfone porous membrane. The influence of the membrane structure and the nature of ILs on the CO<sub>2</sub> capture abilities were investigated. It was found that the membrane's internal morphology and its surface characteristics influence its ILs sorption capacity and CO<sub>2</sub> solubility. In most of the studied configurations, supporting ILs on porous structures increased their contact surface and gas adsorption compared to the bulk ILs. The phenomenon was strongly pronounced in the case of ILs of high viscosity, where supporting them on porous structures resulted in a CO<sub>2</sub> solubility value increase of 10×. Finally, the highest CO<sub>2</sub> solubility value (0.24 mol<sub>CO<sub>2</sub></sub>/mol<sub>IL</sub>) was obtained with membranes bearing supported ILs containing dicarboxylate anion (BMI.MAL).

**Keywords:** CO<sub>2</sub> capture; ionic liquids; supported ionic liquid; gas adsorption



**Citation:** Domingo Huguet, D.; Gual, A.; Garcia-Valls, R.; Nogalska, A. Supported Imidazolium-Based Ionic Liquids on a Polysulfone Matrix for Enhanced CO<sub>2</sub> Capture. *Polymers* **2022**, *14*, 4865. <https://doi.org/10.3390/polym14224865>

Academic Editor: Hailiang Liu

Received: 21 October 2022

Accepted: 8 November 2022

Published: 11 November 2022

**Publisher's Note:** MDPI stays neutral with regard to jurisdictional claims in published maps and institutional affiliations.



**Copyright:** © 2022 by the authors. Licensee MDPI, Basel, Switzerland. This article is an open access article distributed under the terms and conditions of the Creative Commons Attribution (CC BY) license (<https://creativecommons.org/licenses/by/4.0/>).

## 1. Introduction

The continued increase in the world population and its dependence on fossil fuels as an energy source has increased the atmospheric carbon dioxide (CO<sub>2</sub>) concentration. This steady rise in anthropogenic CO<sub>2</sub> emissions from the beginning of the industrial era has increased atmospheric CO<sub>2</sub> from ~280 ppm in 1750 to ~415 ppm in 2020 [1]. CO<sub>2</sub>, among others, is considered a greenhouse gas (GHG) because of its capacity to absorb the infrared range of electromagnetic radiation. This radiation comes from Earth's surface after the irradiation of sunlight, avoiding the dissipation of this energy through the atmosphere to space, leading to an increase in the global temperature. The Intergovernmental Panel on Climate Change (IPCC) set the limit on the rise in global temperature to no more than 1.5 °C by the end of the century. To achieve this purpose, a drastic reduction in CO<sub>2</sub> emissions is required until the total decarbonization of the industry by 2050. Taking a look at the principal industrial CO<sub>2</sub> emitters, refineries, power plants operated by fossil fuels, steel-producing plants, cement plants, and the chemical industry are the main entities responsible for the total greenhouse gas emissions [2,3].

Significant research has been carried regarding the mitigation of CO<sub>2</sub> emissions using various ideas, such as its capture or sequestration in solid adsorbents using porous adsorbents [4].

Storage in underground reservoirs has been proposed as a principal solution, but this can only alleviate the problem without being a final solution. Moreover, issues of underground leakage can be possible, translated to soil contamination and acidification due to the acidic nature of the gas, becoming an even bigger problem [2]. For this purpose,

different strategies have been studied in recent years; for example, the use of liquid absorbent solutions has been explored. The liquid sorbent must exhibit certain characteristics: (1) enhanced CO<sub>2</sub> sorption due to the combination of non-polar domains with high CO<sub>2</sub> solubility (CO<sub>2</sub> adsorption) and polar domains with reactivity towards the acidic molecule of CO<sub>2</sub> (CO<sub>2</sub> absorption), (2) moderate viscosity to facilitate CO<sub>2</sub> diffusion, (3) chemical compatibility with the system components, and (4) low vapor pressure to avoid the loss of the solvent by evaporation [5]. The solvents used at industrial levels are based on basic aqueous solutions, the classical choices being alkanolamines, such as ethanolamine, and potassium hydroxide solutions. These aqueous solutions possess high alkalinity, reacting very quickly with the acidic molecule of CO<sub>2</sub> and forming carbamates or carbonates, depending on the nature of the reactant [6,7]. However, these absorbents present different problems, such as their corrosive nature, the aqueous base of the solution making them volatile, and the high amount of energy required for the post-capture CO<sub>2</sub> desorption from the system in order to use the CO<sub>2</sub>. This desorption is not as chemically favored compared to the sorption process, so a high amount of energy is required to desorb the CO<sub>2</sub> and regenerate the sorbent solution for reuse [6]. To overcome these problems, new solvents, such as ionic liquids (ILs) or deep eutectic solvents (DES), are studied for this purpose because of their high solubility of gases. Among them, the use of ILs has been extensively reported. By definition, ILs are salts with a melting point below 100 °C representing a new class of solvents with a nonmolecular ionic character [8]. Different types of ILs have been reported, including completely inorganic ILs or ILs made up of a combination of organic cation and organic or inorganic anions [9–11]. Among their excellent properties are their negligible vapor pressure, high thermal stability, non-flammability, and stability against air and water, as well as their remarkable tuneability and versatility by simply varying the combination of cations and anions [12,13].

However, the use of large amounts of ILs is undesirable due to parameters related to the process engineering (i.e., viscosity), economic factors (high cost), and sustainability. To overcome these issues, the development of supported ionic liquid systems (SILS) has been extensively reported in the literature, with great success. In many cases, the materials obtained displayed the advantageous properties of the pure ionic liquid systems by using much smaller IL amounts supported onto a second material [14].

The support must be inert to ILs, so as not to alter its CO<sub>2</sub> selectivity, and be mechanically stable. The most suitable candidates, in this case, are polymeric membranes. Polymers are very interesting materials for use as the matrix for the solid support of CO<sub>2</sub> absorbers due to the availability of a variety of monomers, polymerization techniques, and possible additives to ensure the desired chemical and mechanical properties. One of the most used techniques for porous polymeric membrane (PMs) preparation is the phase inversion process. For this procedure, a viscous solution of the desired polymer and a suitable solvent is prepared and cast onto a surface. Finally, it is immersed in a non-solvent bath where the polymer precipitates in the form of a porous flat sheet [15]. One of the characteristics of this procedure is that the internal morphology and the porosity of the obtained membrane can be controlled by preparation conditions (concentration, solvents, non-solvents, temperature, humidity) [16], making it possible to obtain the desired internal structure of the membrane for its application. The only requisite of the procedure is that the solvent and non-solvent must be miscible liquids.

The polymeric materials commercially available and mainly used for the membrane preparation can be seen in Figure 1. Among them, polysulfone (PSU) has been chosen for this work due to its excellent properties, including its: (1) mechanical strength; (2) thermo-stability; (3) chemical stability; (4) relative hydrophobicity; (5) ease of handling [17–19].

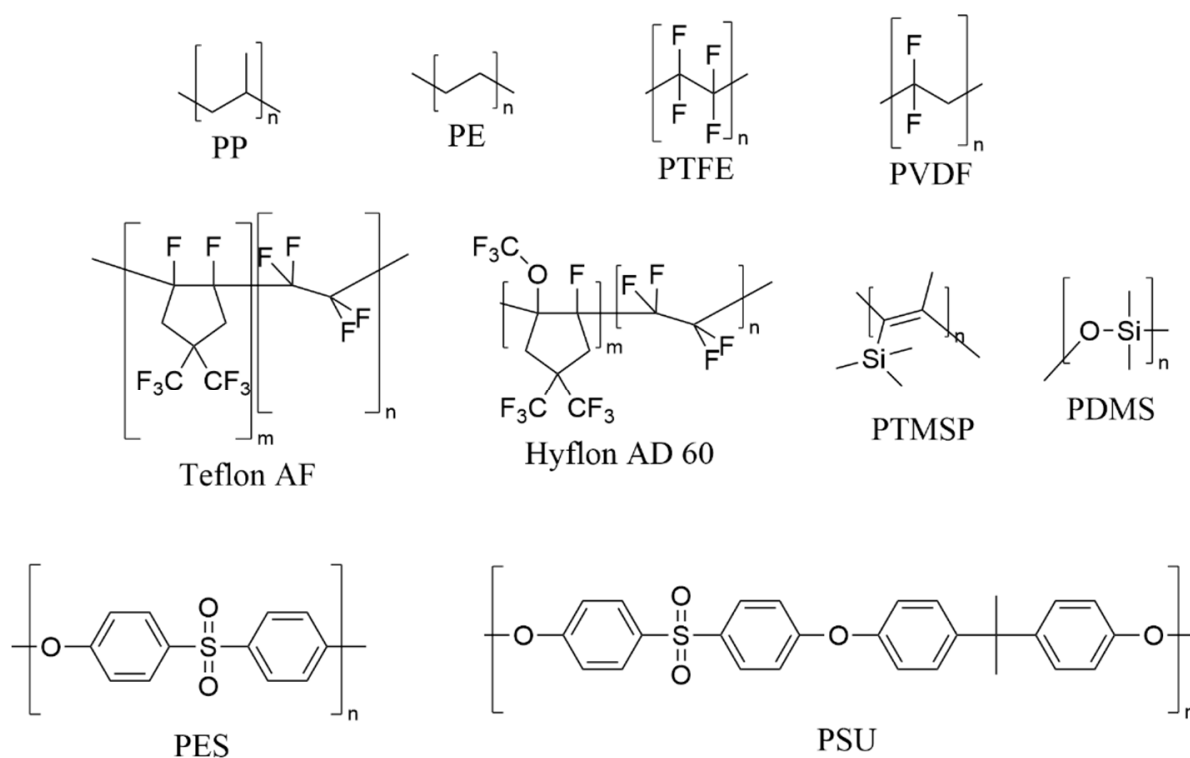
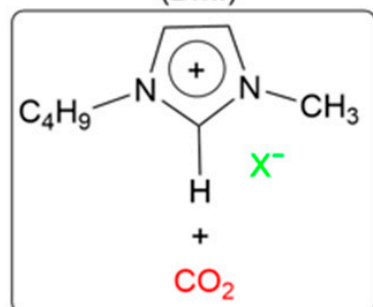


**Figure 1.** Polymer for polymeric membrane preparation; PP: polypropylene; PE: polyethylene; PTFE: polytetrafluoroethylene; PVDF: polyvinylidene fluoride; Teflon amorphous fluoropolymers; Hyflon amorphous perfluoro polymer; PTMSP: poly(1-trimethylsilyl-1-propyne); PDMS: polydimethylsiloxane; PES: polyethersulfone; PSU: polysulfone.

Previous studies have reported good sorption result using the approach of preparing SILs in a polymeric PSU matrix as CO<sub>2</sub> sorption materials [20–22]. In this study, we developed the synthesis of different ILs based on combinations of 1-butyl-3-methyl-imidazolium cations and different anions (BMI·X) for use in the preparation of novel SILs on a polymer porous matrix. Thanks to this approach, we can increase the CO<sub>2</sub> capture rate due to an increased gas/liquid contact area compared to that of bulk ILs and, at the same time, decrease the amount of ILs to be used in this application. Moreover, a solid adsorbent is easier to handle. These IL structures have been selected according to their reported values of CO<sub>2</sub> solubility (Figure 2) (i.e., experimentally measured CO<sub>2</sub> molar fraction in an IL solution of 0.20 to 0.60) [11].

### 1-Butyl-3-methylimidazolium cation (BMI)



X <sup>-</sup>	χ <sub>CO<sub>2</sub></sub>
Chloride	0.23
Bromide	0.25
Acetate	0.53
Proline	0.33
Malonate	0.60

**Figure 2.** CO<sub>2</sub> solubility values reported by the molar fraction of CO<sub>2</sub> at 25 °C and 10 bar [11].

## 2. Materials and Methods

### 2.1. Materials

Polysulfone (PSU, Mw 35,000 Da in transparent pellet form, Sigma Aldrich, St. Louis, MO, USA), *N,N*-Dimethylformamide (DMF, 99% Fisher, Loughborough, UK), and 1-Methyl-2-pyrrolidone (NMP, 99% Acros Organics, New Jersey, NY, USA) were used for membrane preparation.

For the synthesis of 1-butyl-3-methylimidazolium chloride, 1-chlorobutane (99% Acros Organics, Geel, Belgium), 1-methylimidazole (99% Sigma-Aldrich, St. Louis, MO, USA), acetonitrile (CAN, 99.8% Fisher, Loughborough, UK), and ethyl acetate (99.9% VWR, Fontenay-Sous-Bois, France) were used. The task-specific ILs were prepared by the ion exchange process using Amberlite IRA-402(Cl) ion exchange resin (Alfa-Aesar, Kandel, Germany), Sodium hydroxide (NaOH, 97% Fisher, Geel, Belgium), and acidic compounds: benzoic acid (99% Acros Organics, New Jersey, USA), pivalic acid (99% Sigma-Aldrich, Steinheim, Germany), DL-proline (99% Sigma-Aldrich, St. Louis, USA), formic acid (99% Merck, Darmstadt, Germany), and malonic acid (99% Alfa-Aesar, Kandel, Germany)

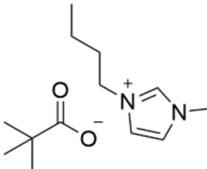
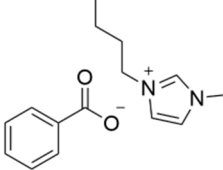
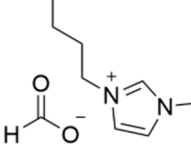
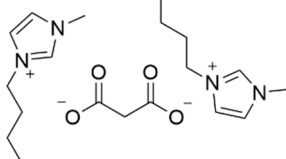
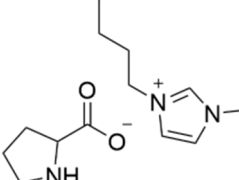
The membrane gas solubility was evaluated with CO<sub>2</sub> (99.995%) and N<sub>2</sub> (99.999%) gases purchased from Linde (Barcelona, Spain).

### 2.2. Ionic Liquids Preparation and Characterization

Ionic liquids have been prepared using procedures adapted from the literature [23]. In a round bottom flask with a double neck, 1-chlorobutane (2.85 mol, 267 g) and 1-methylimidazole (2.85 mol, 237 g) were mixed in a molar ratio of 1:1. The solution was heated under reflux at 90 °C for 72 h while stirring. Next, the unreacted reagents were evaporated under vacuum at 50 °C, and the obtained solid was purified by recrystallization using acetonitrile (500 mL) as a solvent and ethyl acetate (1.5 L) as a crystallization phase. A white crystalline solid was obtained as a product, which was then filtered and dried under vacuum, leading to 1-butyl-3-methylimidazolium chloride (BMI.Cl) with a 90% yield (2.54 mol, 445 g).

Next, the selected ionic liquids were synthesized by an anion exchange using adapted protocols [11]. Using a glass column (3 cm × 50 cm) with 75 g (17 cm) of a Amberlite IRA-402(Cl) ion exchange resin, the chlorine anion of the BMI.Cl was exchanged using conjugated bases of acidic compounds, listed in Table 1, with 3 different groups of compounds; (1) carboxylic acids, (2) dicarboxylic acid, and (3) carboxylic acid with amine compounds. The general procedure for the IL preparation is described below. First, to ensure that all the active sites of the resin were free of chlorine anions, a 1 M solution of NaOH in 200 mL of milliQ<sup>®</sup> water was passed through the column. After that, 1 L of milliQ<sup>®</sup> water was passed to eliminate the excess of hydroxy anions. The procedure was monitored by the pH measurement of the water passed through the resin, resulting in a neutral pH at the end of the process. Then, 0.1 M of 1-butyl-3-methylimidazolium chloride in 500 mL of milliQ<sup>®</sup> water was passed through the column, with an additional 250 mL of milliQ<sup>®</sup> water, to wash out the remaining ionic liquid. Later, the calculated weight of the desired acidic compound was added directly to the aqueous solution and stirred in a 1 L Erlenmeyer for 48 h to ensure the pH equilibrium and the neutralization of the (BMI.OH) by the acid and the formation of the corresponding (BMI.X). Finally, (BMI.X) was dried under reduced pressure, using a rotavapor for 5 h at 80 °C, and using the Schlenck line system for 12 h at 50 °C.

**Table 1.** Synthetized ionic liquids.

Type	Ionic Liquid	Carboxylic Acid Used	Ionic Liquid Structure
1	BMI.PIV	Pivalic Acid (PIV)	
1	BMI.BENZ	Benzoic Acid (BENZ)	
1	BMI.FO	Formic Acid (FO)	
2	BMI.MAL	Malonic Acid (MAL)	
3	BMI.PRO	Proline (PRO)	

Nuclear Magnetic Resonance (NMR) was used to determine the composition of the synthesized ionic liquids. Monodimensional ( $^1\text{H}$ ) experiments were performed in a Bruker Avance Neo 400 MHz spectrometer using deuterium oxide ( $\text{D}_2\text{O}$ ) as a solvent. Chemical shifts (ppm) were provided relative to trimethyl silane (TMS) in  $^1\text{H}$  NMR (16 scans). All ionic liquids purities (>99%) were determined using  $^1\text{H}$  NMR after drying and before its further use.

All ILs were first dried under high vacuum for 4 h at 60 °C before determining the density. Then, using an electronic pipette (Sartorius Picus NxT Electronic Pipette, 50–1000  $\mu\text{L}$ , Goettingen, Germany), 1 mL of IL was collected, and its weight was measured using an analytical scale in triplicate to obtain the ionic liquid density (g/mL). The same procedure was followed for 75% *w/w* in milliQ<sup>®</sup> solutions of ILs, where water was added to dry ILs.

Viscosity measurements were carried out using an IKA Rotavisc Lo-Vi Complete (Staufen, Germany), with an extender connector Vols 1.11, a Spindle Vol SP-6.7, and a sample chamber Vol-C-RTD-1. The viscosity of the ILs solutions used for membrane modification (75% *w/w* ionic liquid in milliQ<sup>®</sup> water) was measured in triplicate. All measurements were carried out at room temperature the same day to ensure similar temperatures for all solutions (21.5–22 °C).

Surface tension was determined using a pendant drop system with a Dataphysics OCA 15EC (Filderstadt, Germany). Ionic liquid 75% *w/w* solutions in milliQ<sup>®</sup> water were placed in a Hamilton de 500/gt syringe (Filderstadt, Germany), and the maximum droop volume was achieved using a manually controlled continuous flow dispenser. All determinations were

carried out in triplicate at room temperature using a digital image created by SCA software (Filderstadt, Germany) included in the apparatus. As a reference, the syringe diameter was obtained, and the density of the solution was determined before measurements.

### 2.3. Membrane Preparation, Ionic Liquids Supporting Methods, and Characterization

A 20% wt. solution of polysulfone in DMF (D\_Membranes) or NMP (N\_Membranes) was prepared by stirring for 48 h. The obtained solution was kept for 24 h without stirring for its degasification and the removal of air bubbles. Membranes were prepared by a phase inversion method, namely by immersion precipitation, at room temperature. The procedure consists of casting the obtained homogeneous solution onto a glass support with a casting knife (gap 200  $\mu\text{m}$ ), followed by its direct immersion into a coagulation bath containing water. Membranes precipitate instantly due to solvent exchange with water (acting as a non-solvent), producing as a product a white, thin, flat porous film that was kept in water for 24 h to ensure complete solvent removal and then dried in air for 48 h before storage.

For the ILs incorporation,  $3 \times 3.5 \text{ cm}^2$  membrane samples were placed in an oven at  $60 \text{ }^\circ\text{C}$  for 72 h. Dry membranes were weighed using an analytical scale (Sartorius ED224S Extend Analytical Balance) and immersed into a 75% *w/w* solution of ionic liquid and milliQ<sup>®</sup> water for 72 h. After that, the membranes were blot dried and placed in the oven at  $60 \text{ }^\circ\text{C}$  for 72 h to ensure water removal and then reweighed (see Table 2). The difference in weight before and after soaking corresponds to the amount of ILs introduced to the membrane.

**Table 2.** Supported ionic liquid membranes.

Classification	Sample	Solvent	Ionic Liquid Cation	Ionic Liquid Anion
D_Membranes	D_PSU	DMF	-	-
	D_BMI.PIV		BMI	Pivalate
	D_BMI.BENZ		BMI	Benzoate
	D_BMI.FO		BMI	Formate
	D_BMI.MAL		2 BMI	Malonate
	D_BMI.PRO		BMI	Prolinate
N_Membranes	N_PSU	NMP	-	-
	N_BMI.PIV		BMI	Pivalate
	N_BMI.BENZ		BMI	Benzoate
	N_BMI.FO		BMI	Formate
	N_BMI.MAL		2 BMI	Malonate
	N_BMI.PRO		BMI	Prolinate

Fourier transform infrared spectroscopy (FT-IR) was used to verify the presence of the ILs in modified membranes and to analyze the membrane after  $\text{CO}_2$  sorption studies. Spectra were obtained using a Bruker Vertex-70 (Madrid, Spain) instrument with an attenuated total reflectance (ATR) sample holder by acquiring 32 cumulative scans with a resolution of  $4 \text{ cm}^{-1}$ .

Physical characterization of the membranes was performed by environmental scanning electron microscopy (ESEM) using a FEI Quanta model 600 electron microscope (Brno, Czech Republic) with a resolution of 3 nm. Membranes were fractured in liquid nitrogen fixed to the suitable support for the cross-section analysis. Morphological characterization was carried out under a low vacuum with a large feed detector (LFD). The ESEM micrographs were recorded with 600 magnifications. Micrographs obtained from ESEM were analyzed with ImageJ software to determine membrane thickness and macrovoid size. Moreover, elemental mapping on the cross-sectional micrographs was obtained using PentaFETx3 Link Dispersive Energy X-ray Spectroscopy (EDXS) managed by Inca Oxford installed in the same equipment.

The supporting membranes porosity (N\_PSU and D\_PSU) ( $\epsilon$ ) was determined from the bulk and the PSU density by using the following Equation (1):

$$\epsilon = \left( 1 - \frac{\rho_m}{\rho_{psf}} \right) * 100\% \quad (1)$$

where  $\rho_m$  and  $\rho_{psf}$  correspond to the membrane and PSU density (1.24 g/cm<sup>3</sup>), respectively [18].

IL interaction with the membrane surface was determined by contact angle measurement with a Dataphysics OCA 15EC. MilliQ<sup>®</sup> water and 75% *w/w* solutions of ionic liquid in MilliQ<sup>®</sup> water were placed in a Hamilton de 500/*gt* syringe. A 3  $\mu$ L droplet of the studied liquid was placed on the top and bottom surface of each membrane type, as both surfaces were in contact with the soaking solution. The contact angle was calculated from a digital image using the SCA software included in the apparatus as the average of 3 measurements.

The membrane surface roughness was analyzed by atomic force microscopy (AFM) using an Agilent 5500 Scanning Probe Microscope in contact mode with a Multi 75 Al-G Budget Sensors tip (resonance frequency 75 kHz and force constant 3 N/m) combined with WsxM software [24]. The surface roughness parameters of the membranes expressed in terms of mean roughness ( $R\alpha$ ) and root mean square of Z ( $Rq$ ) were obtained by a roughness analysis calculated by the software.

#### 2.4. CO<sub>2</sub> Sorption Studies

The CO<sub>2</sub> solubility in the obtained membranes was determined by its pressure decay in a closed chamber. All tests were carried out in a stainless-steel reactor of 50 mL volume with a glass filler to reduce the total volume of the system to 28 mL. All experiments were performed at 30 °C to ensure reproducibility. The pressure was acquired by an electronic manometer (STORKSolutions, model UPS-HSR-B02P5G, range –1 to 2.5 bar). The system used for the CO<sub>2</sub> sorption studies is depicted in Figure 3 (real image in Figure S1 in Supplementary Materials). The procedure for conducting the experiments is as follows. The membrane (3 × 3 cm<sup>2</sup>), previously dried at 60 °C for 72 h and stored under non-humidity ambient conditions until ambient temperature, was introduced into the reactor. Then, the reactor was immersed in the water bath. After temperature stabilization, the system was purged with 2 barg of pure N<sub>2</sub> three times to ensure complete air removal from the reactor volume. The next step was pressurizing the system to 2 bar by closing the valves with pure N<sub>2</sub> for 30 min until pressure stabilization was reached to confirm its hermeticity. Then, the system was depressurized, purged, and charged with pure CO<sub>2</sub> to 2 barg. The pressure decay was monitored for 5 h. Finally, the system was vented and the membrane extracted for further characterization with ATR-IR. Blank experiments were conducted using N<sub>2</sub> instead of CO<sub>2</sub>.

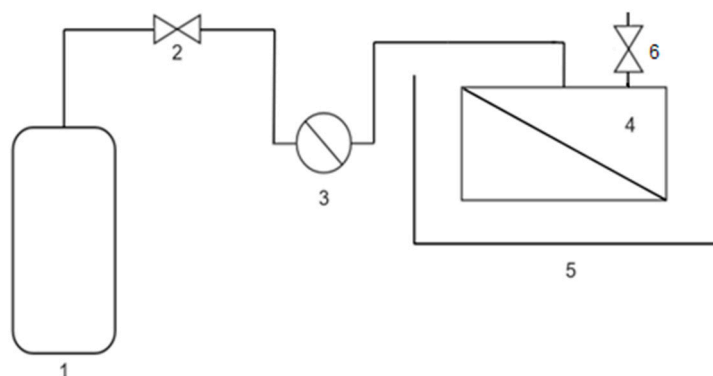


**Figure 3.** Solubility system: (1) CO<sub>2</sub> bottle; (2) valve to close the system; (3) electronic manometer; (4) reactor containing membrane; (5) water bath at 30 °C; (6) exit valve.

The solubility coefficient is given in  $\text{m}^3$  of gas at standard conditions (1 atm and 273.15 K (STP)) per  $\text{m}^3$  of membrane conditions, obtained by the following Equation (2):

$$S = \frac{V_{stp}}{V_m * P_f} \quad (2)$$

where  $S$  corresponds to the solubility coefficient [ $\text{m}^3$  (STP)  $\text{m}^{-3}$  membrane  $\text{atm}^{-1}$ ],  $V_{stp}$  is the volume of  $\text{CO}_2$  adsorbed in STP [ $\text{m}^3$ ],  $V_m$  corresponds to membrane volume [ $\text{m}^3$ ], and  $P_f$  to the final pressure of the system after stabilization [atm].

Further, the  $\text{CO}_2$  sorption was recalculated to moles of  $\text{CO}_2$  adsorbed per mol of IL to normalize and compare the results. The  $\text{CO}_2$  solubility in the unmodified PSU membrane (D\_PSU  $6.28 \times 10^{-5}$  mol  $\text{CO}_2$ /g PSU and N\_PSU  $2.8 \times 10^{-4}$  mol  $\text{CO}_2$ /g PSU) was subtracted in order to study the influence of supporting the ILs on its  $\text{CO}_2$  sorption capacity. The adsorbed  $\text{CO}_2$  moles were determined following Equation (3):

$$n\text{CO}_2 = \frac{(P_i - P_f) \times (V_v - V_m)}{R \times T} \quad (3)$$

where  $n\text{CO}_2$  corresponds to adsorbed  $\text{CO}_2$  moles [mol],  $P_i$  and  $P_f$  correspond to the initial and final pressure [Pa], respectively,  $V_v$  is the volume of the empty chamber (gas volume) [ $\text{m}^3$ ],  $V_m$  is the volume of analyzed material [ $\text{m}^3$ ],  $R$  is the gas constant ( $8314 [\text{m}^3 \cdot \text{Pa} \cdot \text{K}^{-1} \cdot \text{mol}^{-1}]$ ), and  $T$  is the temperature [K]. The volume of the material was measured based on the correlation between the PSU volume, taking into account the membrane porosity and ILs volume in each membrane calculated from the mass increase, and the density of the ILs.

### 3. Results

#### 3.1. Synthesized Ionic Liquids

Following the procedure listed in 2.2, a white crystalline solid was obtained as a product, which was then filtered and dried under vacuum leading to 480 g of 1-butyl-3-methylimidazolium chloride (BMI.Cl) with a 96% yield. The product was characterized by  $^1\text{H}$  NMR (see Figure S2 in Supplementary Materials). After BMI.Cl obtention, the anion exchange was performed to acquire the desired task-specific ILs (Table 2). The anion exchange process provided the IL structures in quantitative yields (>99%). The products obtained displayed the expected signals in the  $^1\text{H}$  NMR spectra (see Figures S3–S7 in Supplementary Materials) and IR spectra (see Figures S8–S13 in Supplementary Materials).

The prepared ILs were divided into 3 groups to study the influence of different anions of the BMI.X on the  $\text{CO}_2$  capture rate: (1) ILs bearing carboxylate anions (BMI.FO, BMI.PIV, and BMI.BENZ), (2) ILs bearing dicarboxylate anion (BMI.MAL), and (3) ILs bearing carboxylate anions containing amine (BMI.PRO).

#### 3.2. Physio-Chemical Characterizations of Membranes

To determine the efficiency of the incorporation of ILs in the membranes of different internal morphologies and to study their  $\text{CO}_2$  adsorption capabilities, two blank membranes were prepared (D\_Blank and N\_Blank) and used as a support for 5 different ILs. A total of 12 different membranes were prepared (Table 2).

The internal membrane morphology was determined by a cross-sectional study using environmental scanning electron microscopy (ESEM). Figures 4 and 5 show the obtained micrographs. As can be seen, the internal structure of the D\_Membranes (Figure 4) was filled with micropores and macrovoids with a drop-like structure, while the N\_Membranes (Figure 5) were filled with macrovoids of finger-like structure. This morphology changes because of the solvent used for polymeric solution preparation due to different interaction of the solvents with water when the casted polymeric solution was immersed into the coagulation bath during membrane preparation. The polymer precipitation velocity is one



of the key factors responsible for the final membrane morphology. The faster the penetration of the coagulation agent, the higher the asymmetry obtained, including more elongated macrovoids and a thicker membrane. Several parameters influence the precipitation velocity, such as precipitation kinetics, polymeric solution viscosity, and the thickness of the casting knife.

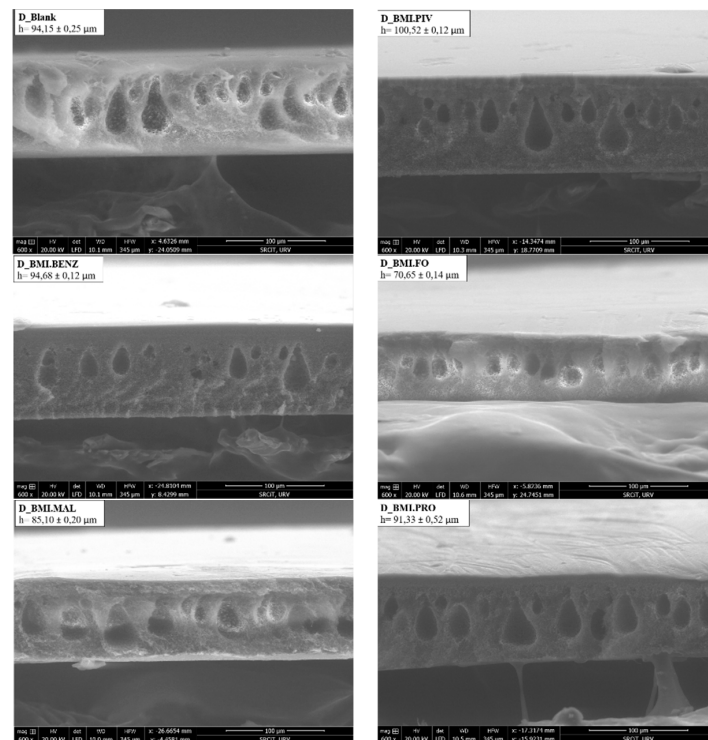


Figure 4. ESEM micrographs of the DMF membranes.

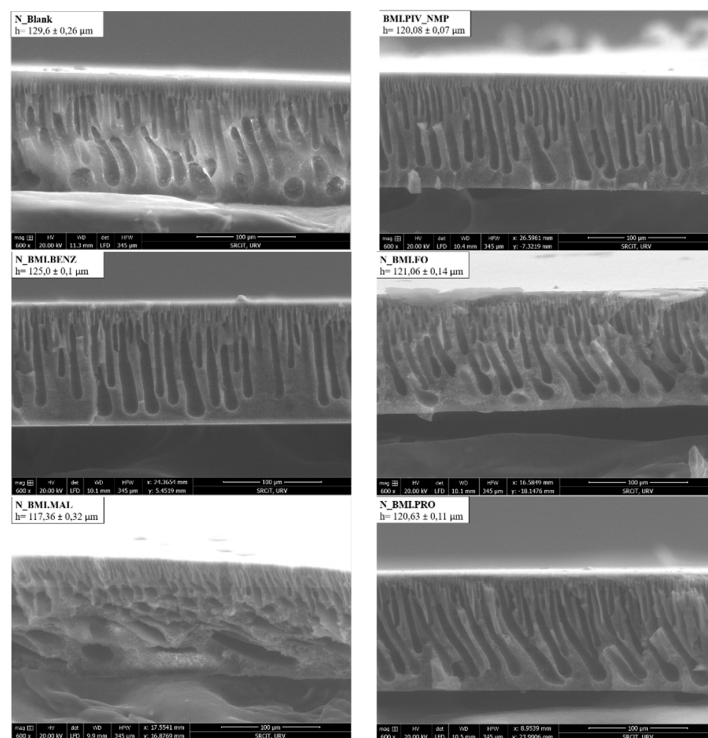


Figure 5. ESEM micrographs of the NMP membranes.

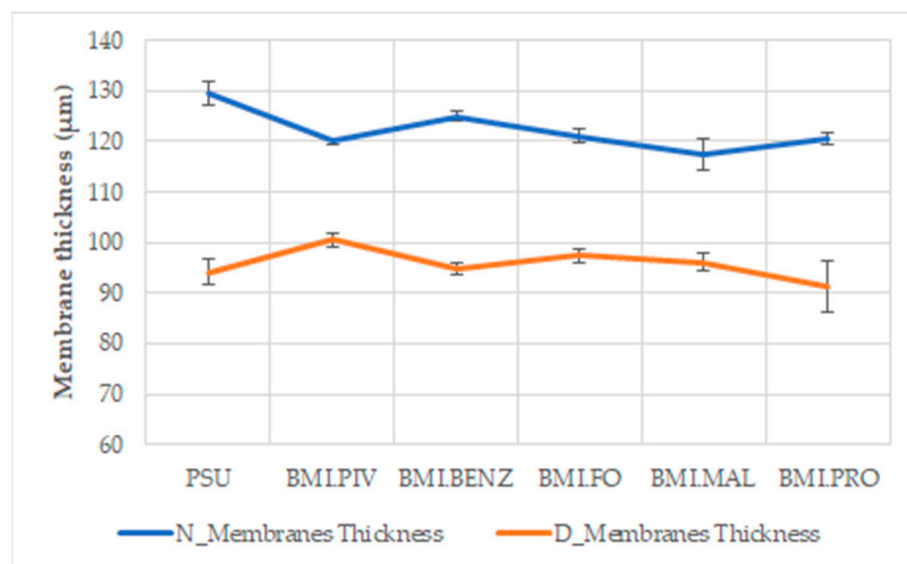
Comparing the images of blank membranes with the ones obtained from the membranes containing ILs, we confirmed that no structural changes in the membrane were induced by incorporating ILs into its structure. The authors suspect that the ILs were adsorbed only by physical interactions.

Table 3 shows the membrane preparation conditions and the obtained membrane characteristics. In our case, a higher thickness value was obtained with N\_Membranes. Such membranes show an internal morphology mainly composed of an asymmetric fingerlike structure on the top portion due to a faster polymer precipitation. The N\_Membranes exhibit a higher porosity and thickness, but a lower macrovoid size than the D\_Membranes.

**Table 3.** Membrane preparation conditions and characteristics.

	D_Blank	N_Blank
Process	Immersion precipitation	
Polymeric Solution	20% w/w of polysulfone	
Solvent	DMF	NMP
Casting Knife ( $\mu\text{m}$ )	200	
Support	Glass	
Membrane Thickness ( $\mu\text{m}$ )	$94.1 \pm 0.2$	$129.6 \pm 0.3$
Porosity (%)	67	73
Macrovoid size ( $\mu\text{m}$ )	$32 \pm 7$	$15 \pm 4$

The membrane thickness has also been examined in the membranes with ILs to determine if the soaking process promotes an expansion of the membrane, increasing the thickness. Figure 6 shows that the membrane thicknesses for the N\_Membranes have similar values (between 130  $\mu\text{m}$  and 115  $\mu\text{m}$ ), and the same applies to the D\_Membranes (between 90  $\mu\text{m}$  and 100  $\mu\text{m}$ ).



**Figure 6.** Membrane thickness after soaking, as measured by ESEM analysis.

### 3.2.1. Infrared Studies (IR)

IR studies were performed to confirm the presence of ionic liquids in the membranes. Figures 7 and 8 show a part of the stacked IR spectra in which the unmodified membrane (D\_PSU and N\_PSU), the corresponding ionic liquid (BMI.BENZ), and the modified membrane (D\_BMI.BENZ and N\_BMI.BENZ) can be seen. The most characteristic bands that can confirm the presence of ionic liquids in the membrane were the ones that correspond to the stretching of C-N (from the cation) that can be seen at around  $1640\text{ cm}^{-1}$ , and the presence of bands corresponding to the symmetrical and asymmetrical stretching carbonyl simple

bond (from the carboxylate anions) that can be seen at around  $1360\text{ cm}^{-1}$  and  $1570\text{ cm}^{-1}$ , respectively. No new chemical bonds between the ionic liquid and the PSU have been detected, confirming that the ionic liquids were physically incorporated into the membrane by pore and macrovoid filling and not by chemical reaction. Even though the ATR-IR only penetrates the first  $4\text{ }\mu\text{m}$  of the membrane, we were able to confirm the presence of ILs in the membrane structure. (For all spectra, see Figures S14–S23 in Supplementary Materials).

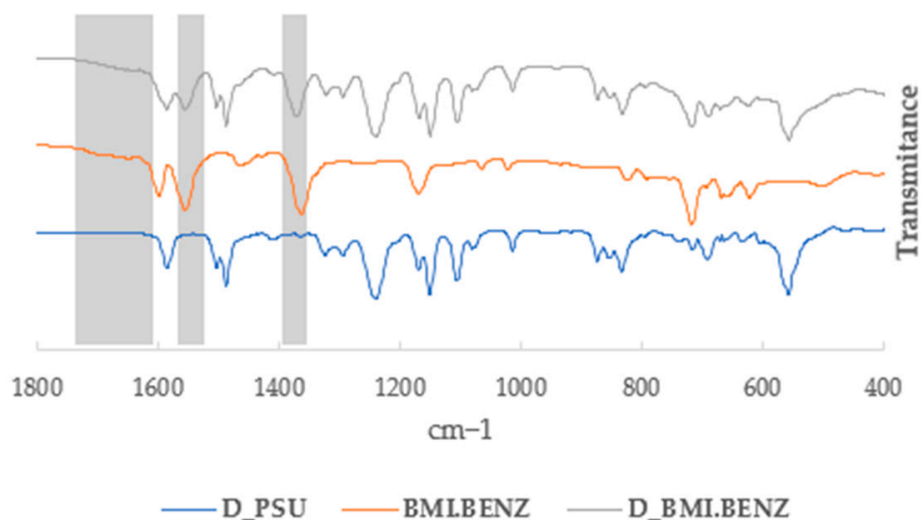


**Figure 7.** Partial IR spectra of D\_PSU, BMI.BENZ IL, and D\_BMI.BENZ.

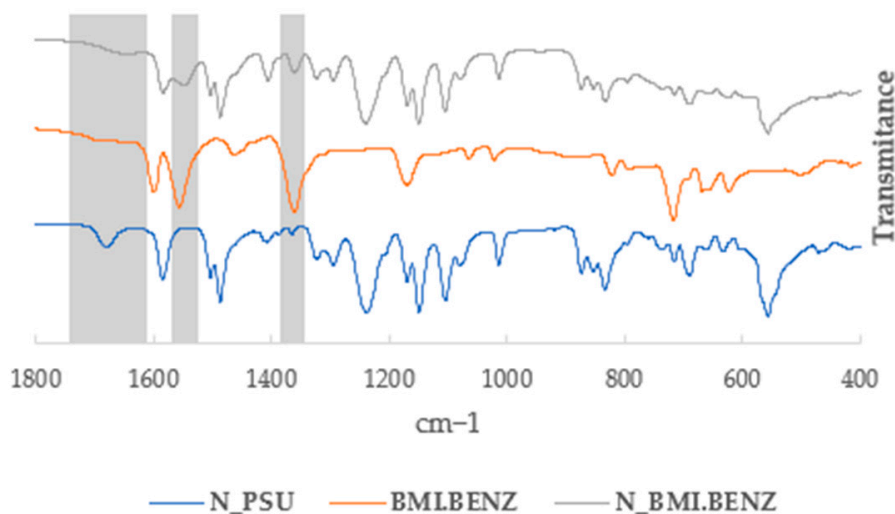


**Figure 8.** Partial IR spectra of N\_PSU, BMI.BENZ IL, and N\_BMI.BENZ.

### 3.2.2. Energy Dispersive X-ray Elemental Analysis

The energy dispersive X-ray elemental analysis was performed on the cross-section of the membranes. The presence of nitrogen inside the membranes was assigned to the imidazolium cation and confirmed the presence of an ionic liquid. Figure 9 shows an example of elemental analysis characterization, the D\_BMI.BENZ membrane cross-section, which highlighted a good dispersion of nitrogen (blue) all along the membrane and confirmed the presence of ionic liquids inside the membrane. It must be noted that the ionic liquid was well dispersed and not concentrated in the macrovoids (for all micrographs, see Figures S24–S35 and Tables S1–S12 in Supplementary Materials). Besides the nitrogen, carbon, sulfur, and oxygen was found to be present, mainly in PSU structure.

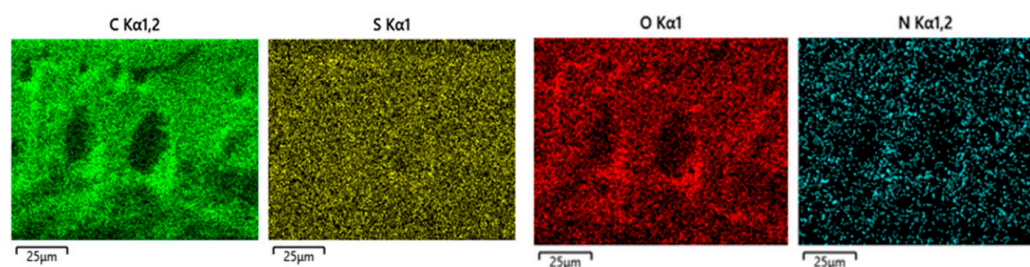


**Figure 9.** EDX analysis of D\_BMI.BENZ.

### 3.3. Sorption of the ILs into Membrane Pores by Capillary Forces

#### 3.3.1. Mass Increase Determination

The amount of ILs introduced into the membrane was determined by the mass change before and after the soaking process. Figures 10 and 11 display the results of the mass increase (%) obtained for the membranes of different structures.

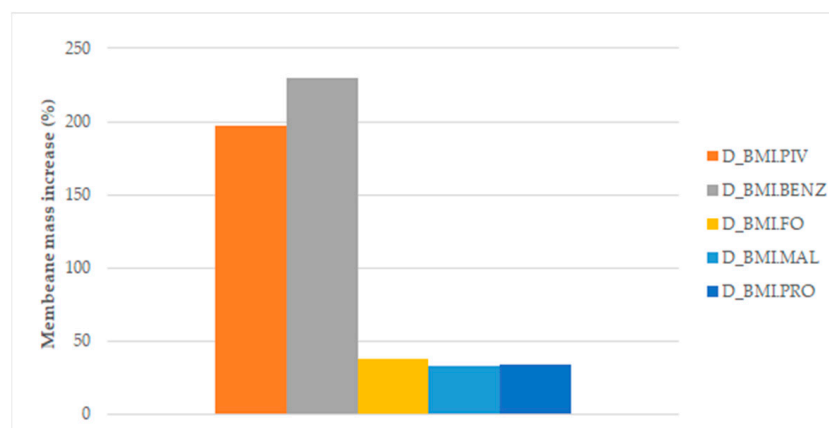


**Figure 10.** Mass increase after soaking the DMF membranes.

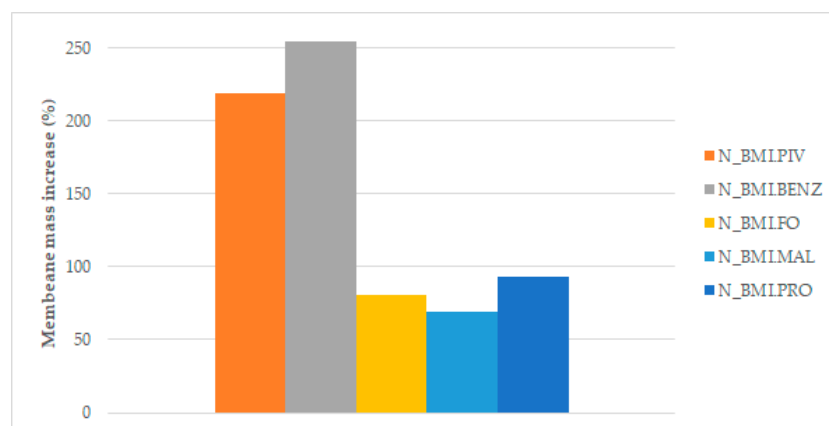


**Figure 11.** Mass increase after soaking the NMP membranes.

As can be seen in Figures 10 and 11, the best adsorption of IL in the membrane was achieved with BMI.PIV and BMI.BENZ in both types of membranes. In these two cases, the mass increase rose to values near 200% for the D\_Membranes and 250% for the N\_Membranes, while for the other ILs, the increase was lower than 50% for the D\_Membranes and lower than 90% for the N\_Membranes, indicating that these ionic liquids can be efficiently adsorbed. This behavior has been ascribed to the higher affinity of the relatively hydrophobic polysulfone polymer by the ILs with more hydrophobic character, such as BMI.PIV, and those ILs with aromatic anions, such as BMI.BENZ, could plausibly cause  $\pi$ - $\pi$  stacking interactions with polysulfone aromatic rings.

As expected, the best adsorption results were obtained with the N\_Membranes for all the studied ILs. The introduction of the ILs to the membrane pores by soaking is based on capillary action. Capillary action is explained by Jurin's law, which states that the maximum high ( $h$ ) of a liquid in a capillary tube is inversely proportional to the tube diameter. If the diameter of the tube (in our case, of the macrovoid) is sufficiently small, then the combination of surface tension and adhesive forces between the liquid and the pore wall act to propel the liquid. The law is defined by the following equation:

$$h = \frac{2\gamma\cos\theta}{\rho gr} \quad (4)$$

where  $h$  corresponds to the height of a liquid in a column (macrovoids),  $\gamma$  to the surface tension of each ILs (mN/m),  $\rho$  to the density of the ionic liquid (g/mL),  $g$  to the local acceleration due to gravity,  $r$  to the tube or macrovoids radius, and  $\theta$  is the contact angle between the membrane and the ILs. Based on the capillary action theory, the N\_Membranes should exhibit a higher efficiency of ILs sorption, as it has a higher contact angle ( $\cos \theta$ , Figure 15) and a lower macrovoid size ( $r$ , Table 3). Moreover, the N\_Membranes have a higher porosity and thickness (Table 3), which allows them to retain higher volumes of ILs.

As the incorporation of the ILs was achieved mainly by capillary forces, it has been attempted to correlate the difference in soaking efficiency among the ionic liquids used with the viscosity of the ionic liquids, or rather the viscosity of the solutions used for soaking (75%wt), their density, and their surface tension. It was expected that a higher solution surface tension ( $\gamma$ ) or lower density ( $\rho$ ) would result in a higher quantity of ILs introduced to the membrane. However, no direct correlation has been discovered. All obtained values can be found in SP (specifically Tables S13–S15 in Supplementary Materials).

### 3.3.2. Membrane Roughness Determination

Membrane roughness also plays a role in the absorption efficiency of the ionic liquids. Figures 12 and 13 show a 3D representation of the D\_PSU and N\_PSU membrane surfaces, respectively. In the images, it can be seen that the top surfaces were more homogeneous those on the bottom, in both cases.

Table 4 includes the roughness values obtained for both types of supporting membranes used in this work. D\_PSU has similar Ra and Rq values for both surfaces, while the surfaces of N\_PSU were diverse, as the top surface was 5 times rougher than the bottom surface. Moreover, comparing the roughness of each surface between the membranes, it can be seen that N\_PSU has higher values for the top surfaces and D\_PSU for the bottom surfaces.

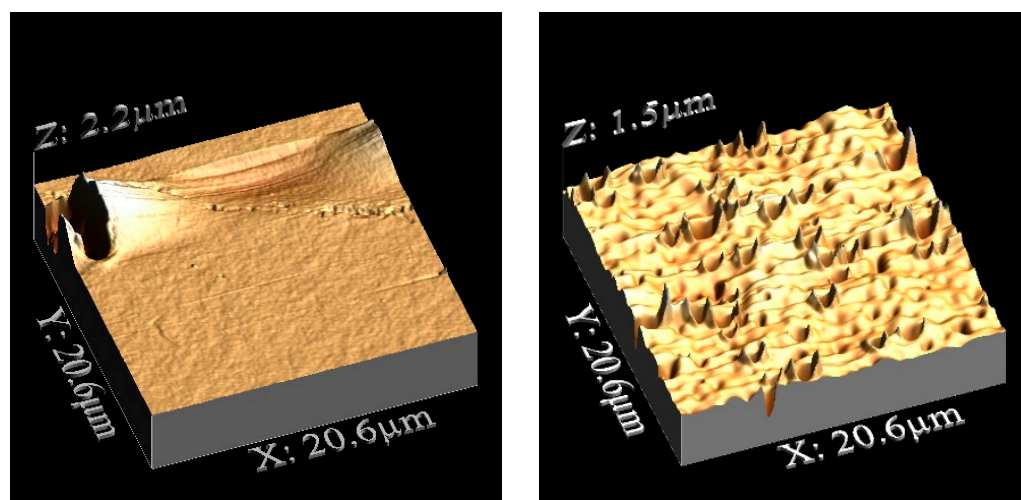


Figure 12. (Left) AFM top surface, D\_PSU. (Right) AFM bottom surface, D\_PSU.

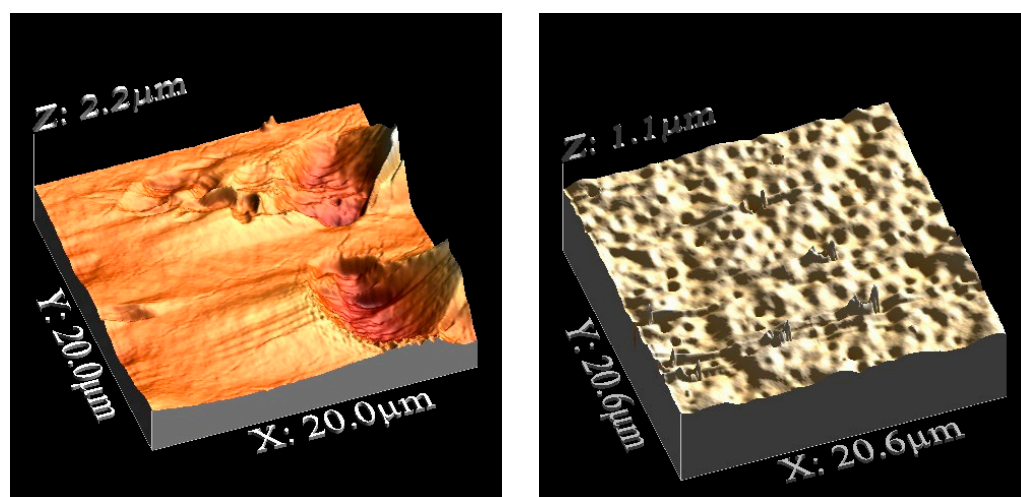


Figure 13. (Left) AFM top surface, N\_PSU. (Right) AFM bottom surface, N\_PSU.

Table 4. Atomic force microscopy results for D\_PSU and N\_PSU membranes.

Membrane	Surface	Average Roughness (Ra)	Root Mean Square (Rq)	Skewness
D_PSU	Top	$0.05 \pm 0.6$	$0.13 \pm 0.08$	−0.84
D_PSU	Bottom	$0.0654 \pm 0.007$	$0.106 \pm 0.004$	−2.29
N_PSU	Top	$0.16 \pm 0.04$	$0.21 \pm 0.02$	0.27
N_PSU	Bottom	$0.027 \pm 0.005$	$0.041 \pm 0.002$	−3.69

In addition, the skewness of the membranes was studied to provide more information about the membrane surfaces. Positive values correlate with surfaces where the roughness was constituted by hills, while negative values correspond to a surface with more valleys. The membrane prepared with NMP (N\_PSU) was the only one among all the membranes studied that presented a positive skewness value on its top surface. The positive skewness value can be related to facilitated capillary action and may contribute to the higher mass increase during the membrane soaking.

### 3.3.3. Contact Angle Determination

In order to determine the influence of the surface–liquid interaction on the ionic liquid absorption behavior, contact angle experiments were carried out on the bottom and top surfaces of the supporting membranes and soaking solutions. Figures 14–16 show the results obtained for the CA measurements, including milliQ<sup>®</sup> water as a reference and the membrane mass increase after soaking (for contact angle images, see Figures S36–S59 in Supplementary Materials). All values of CA are below 90°, which indicates that the surfaces were IL-philic. Thus, they will adsorb ILs or will let them pass. We demonstrated that the lower the contact angle between the soaking solution and the membrane, the more efficient the soaking procedure. As can be seen in Figures 14 and 15, corresponding to the top surfaces of both membranes, the solutions that have the lowest CA were the ones prepared with BMI.PIV and BMI.BENZ; thus, they ones that resulted in the highest mass increase. Nevertheless, no differences in the CA values were observed between the bottom surfaces (Figures 16 and 17), suggesting that the ILs absorption could be mainly influenced by the properties of the top surface of the membranes.

As for the influence of the membrane type, in general, lower contact angles were obtained with the membranes prepared with DMF as a solvent, but a higher mass increase was obtained with the membranes prepared with NMP. However, as previously mentioned, due to lower macrovoid size, stronger capillary forces act on the N\_Membranes, and therefore, the membrane was more predisposed to adsorb higher amounts of ILs.

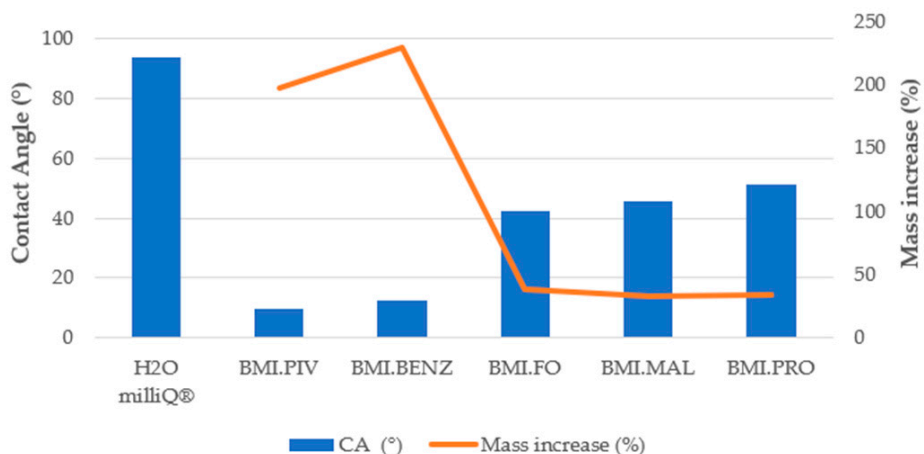


Figure 14. Top surface contact angle and membrane mass increase correlation for the D\_Membranes.

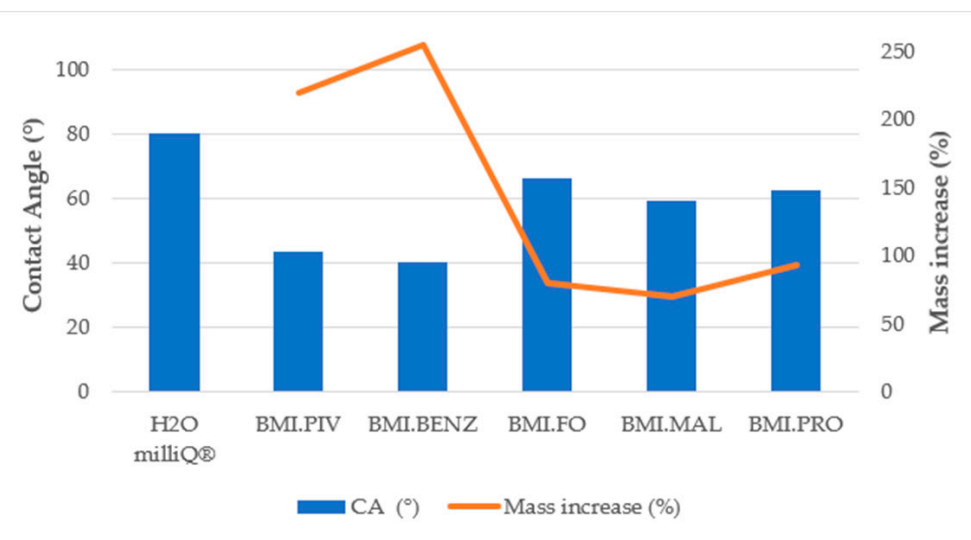


Figure 15. Top surface contact angle and membrane mass increase correlation for the N\_Membranes.

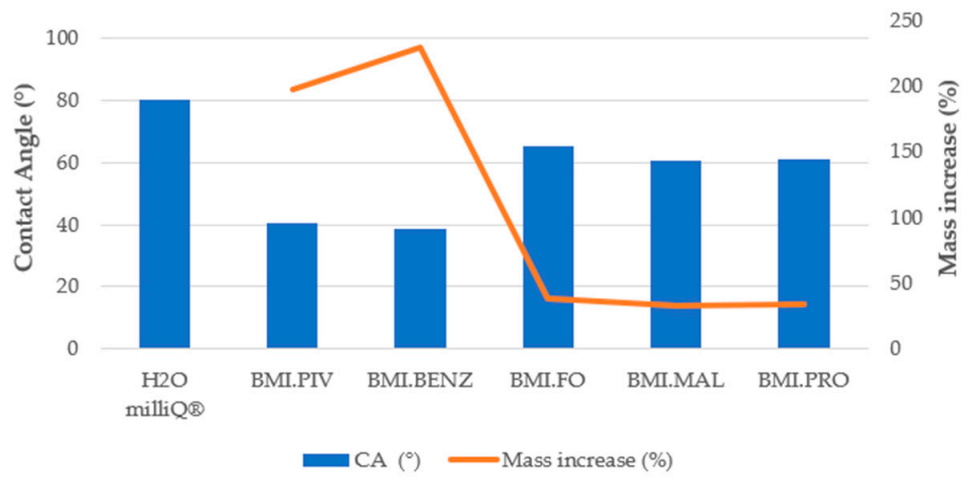
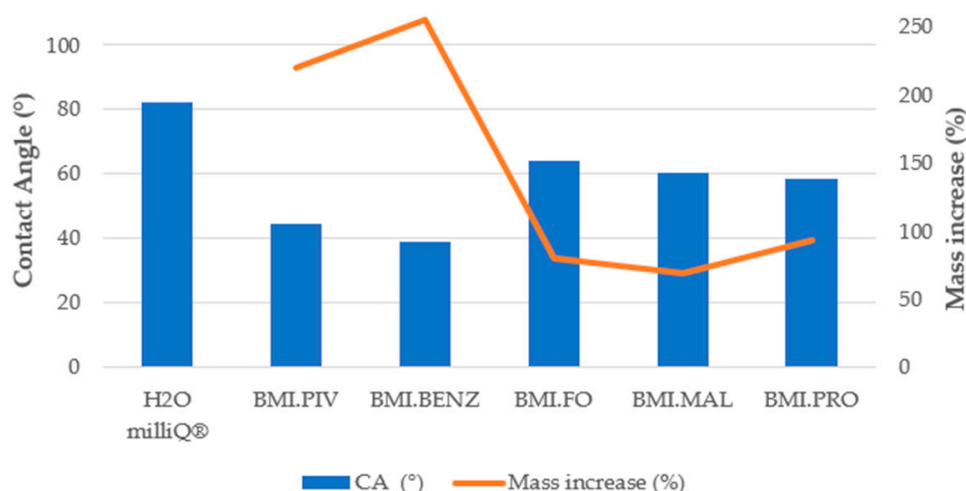


Figure 16. Bottom surface contact angle and membrane mass increase correlation for the D\_Membranes.



**Figure 17.** Bottom surface contact angle and membrane mass increase correlation for the N\_Membranes.

Based on the soaking studies and the characterization of both types of membranes, we can conclude that in general better membranes for IL absorption using the soaking method were the N\_Membranes due to their high porosity and top surface properties.

### 3.4. Solubility Results

The sorption of N<sub>2</sub> and CO<sub>2</sub> of all the studied samples was evaluated; however, no sorption was detected in the case of N<sub>2</sub>. These results suggest a >99% selectivity for CO<sub>2</sub> sorption. Table 5 shows the results obtained for CO<sub>2</sub>. Nevertheless, an increase in CO<sub>2</sub> sorption capabilities by at least one order of magnitude was achieved for all modified membranes in comparison to the pristine PSU membranes (Table 5). However, the results obtained for each ILs are not comparable, as different amounts were introduced to the membrane support.

**Table 5.** Solubility coefficients obtained by Equation (2).

Membrane	Solubility Coefficient (S) (m <sup>3</sup> (STP) m <sup>-3</sup> <sub>membrane</sub> atm <sup>-1</sup> )
D_PSU	4.16 × 10 <sup>4</sup>
D_BMI.PIV	5.25 × 10 <sup>6</sup>
D_BMI.BENZ	2.72 × 10 <sup>6</sup>
D_BMI.FO	2.03 × 10 <sup>5</sup>
D_BMI.MAL	1.31 × 10 <sup>5</sup>
D_BMI.PRO	7.27 × 10 <sup>4</sup>
N_PSU	1.83 × 10 <sup>5</sup>
N_BMI.PIV	7.30 × 10 <sup>11</sup>
N_BMI.BENZ	3.40 × 10 <sup>11</sup>
N_BMI.FO	5.08 × 10 <sup>5</sup>
N_BMI.MAL	1.05 × 10 <sup>6</sup>
N_BMI.PRO	2.52 × 10 <sup>6</sup>

For another point of view, CO<sub>2</sub> solubility was determined to assess the direct effect of supporting the ILs in a PSU matrix. These results were obtained by normalizing the absorbed CO<sub>2</sub> moles in the supported ionic liquid by the subtraction of CO<sub>2</sub> sorption in the blank membranes to obtain the mol of CO<sub>2</sub> sorbed by the mol of the IL (see Section 2.4). In general, the CO<sub>2</sub> sorption results (Figure 18) revealed an enhancement of the IL sorption capacity by the use of polysulfone as a polymeric matrix for its support. This behavior could be ascribed to an expansion of the contact between the ILs and the gas. The numerical



values obtained for the CO<sub>2</sub> moles adsorbed and their solubility can be found in Tables S16–S18 in Supplementary Materials.

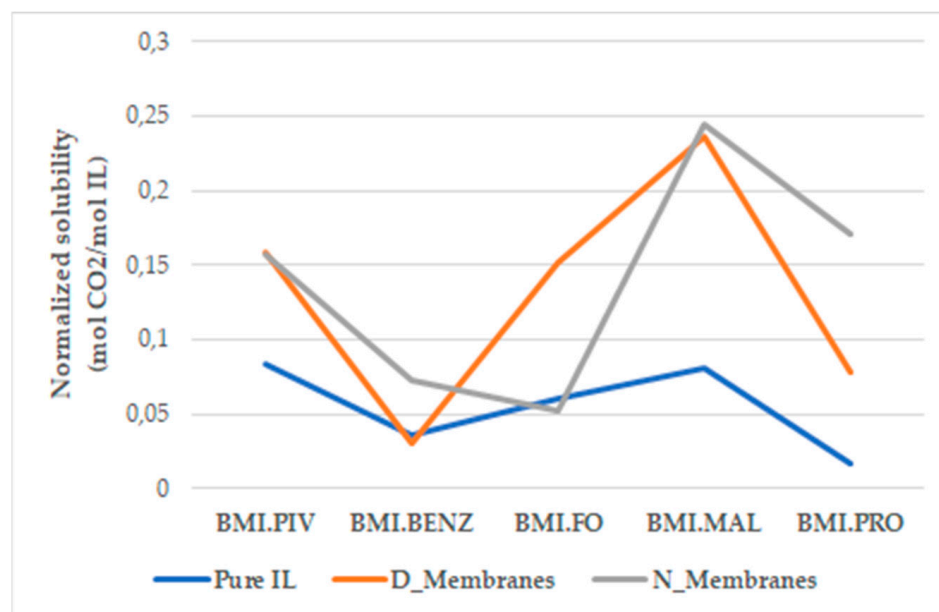


**Figure 18.** Solubility results for bulk ionic liquids and supported ionic liquids.

As previously mentioned, the ILs used in this work were divided into three groups, and different improvements were established for each type. The first one (Type 1) contains a carboxylate anion and exhibits different behaviors for each compound. The best solubility among this group was obtained with BMI.PIV, supported in both membrane types, doubling the CO<sub>2</sub> solubility. Taking into account that this IL was introduced in high amounts to the membranes, it also shows the highest capacity of total CO<sub>2</sub> adsorption per surface of the membrane. While BMI.FO was supported in the N\_Membranes and BMI.BENZ in the D\_Membranes, these membranes were the only ones that exhibited roughly the same CO<sub>2</sub> sorption as the bulk ionic liquid.

The second type of ionic liquid, the one containing the dicarboxylate anion (Type 2), yielded the highest adsorption value for both supported and unsupported ILs among all studied systems. The values obtained for supported BMI.MAL were twice as high as those for the unsupported one, reaching 0.24 molCO<sub>2</sub>/mol<sub>IL</sub>.

The third type of ILs was the one containing an amine group in the anion BMI.PRO (Type 3). In this case, the CO<sub>2</sub> solubility studies showed the lowest efficiency in the bulk ILs. However, when supported, the value increased 10 times. This IL has the highest viscosity among those tested; thus, by supporting it, we were able to increase the contact surface area and thereby, increase the diffusion, as it is directly connected to the viscosity by the Stokes–Einstein law. This suggests that the use of a porous membrane to support ILs in order to improve their CO<sub>2</sub> capture rate will have the highest impact in highly viscous ILs.

The ILs supported on membranes made with NMP (N\_Membranes) yielded better results in most cases, due to the higher porosity of the membrane compared to that of the D\_Membranes, as well as the same or better ILs distribution. A positive synergistic effect between the IL and the PSU matrix was found that improved the CO<sub>2</sub> sorption capacities of both ILs and the membranes.

In order to determine the type of sorption present in our CO<sub>2</sub> capturing system, ATR-IR analysis were carried out after the solubility studies. Since the obtained spectra did not show the creation of a carbamate bond, a physical CO<sub>2</sub> sorption must be expected. However, chemical CO<sub>2</sub> sorption in ILs cannot be discounted due to the low amount of the ILs compared to the PSU matrix, which could quench the new IR bands formed by the low amount of CO<sub>2</sub> chemically incorporated into the membranes.

#### 4. Conclusions

N\_Membranes can uptake more ILs than D\_Membranes, due to a higher free volume inside the membrane resulting from its porosity and thickness. Additionally, its characteristics, such as positive skewness or smaller macrovoids size, affect the strength of capillary action and provide an uptake advantage.

The incorporation of ILs was demonstrated by the mass change after soaking experiment and by the ATR-IR and ESEM-EDX analysis. Moreover, the incorporation was found to be physical, which is supported by ATR-IR studies, and it did not affect the membranes' internal morphologies nor thicknesses.

The amount of the ILs introduced into the membrane depends on the membrane porosity and the ILs interaction with its surface, especially the contact angle. The ionic liquids BMI.PIV and BMI.BENZ were found to have the lowest contact angle on the polysulfone membranes, which allowed for easier penetration.

The CO<sub>2</sub> solubility was improved when ILs were supported into porous membranes thanks to improvement in the contact area between the liquid and gas. This phenomenon was specially noted with ILs of high viscosity where dispersion of ILs in the pores caused a more pronounced improvement in diffusion. The best results were obtained with BMI.MAL, which possesses a double carboxylate anion. Finally, we can confirm that the N\_Membranes were the most suitable in terms of ILs uptake and CO<sub>2</sub> solubility improvement. A positive synergistic effect between the IL and the PSU matrix was found, which improved the CO<sub>2</sub> sorption capacities of both the ILs and the membranes.

**Supplementary Materials:** The following supporting information can be downloaded at: <https://www.mdpi.com/article/10.3390/polym14224865/s1>, Figure S1. Real set-up for solubility experiments, Figure S2. <sup>1</sup>HNMR spectra of compound 1, Figure S3. <sup>1</sup>HNMR spectra of compound 2, Figure S4. <sup>1</sup>HNMR spectra of compound 3, Figure S5. <sup>1</sup>HNMR spectra of compound 4, Figure S6. <sup>1</sup>HNMR spectra of compound 5, Figure S7. <sup>1</sup>HNMR spectra of compound 6, Figure S8. IR spectra of compound 1 (BMI.Cl), Figure S9. IR spectra of compound 2 (BMI.PIV), Figure S10. IR spectra of compound 3 (BMI.FORM), Figure S11. IR spectra of compound 4 (BMI.BENZ), Figure S12. IR spectra of compound 5 (BMI.PRO), Figure S13. IR spectra of compound 6 (BMI.MAL), Figure S14. IR stacked spectra D\_PSU, BMI.PIV and D\_BMI.PIV, Figure S15. IR stacked spectra D\_PSU, BMI.BENZ and D\_BMI.BENZ, Figure S16. IR stacked spectra D\_PSU, BMI.FO and D\_BMI.FO, Figure S17. IR stacked spectra D\_PSU, BMI.MAL and D\_BMI.MAL, Figure S18. IR stacked spectra D\_PSU, BMI.PRO and D\_BMI.PRO, Figure S19. IR stacked spectra N\_PSU, BMI.PIV and N\_BMI.PIV, Figure S20. IR stacked spectra N\_PSU, BMI.BENZ and N\_BMI.BENZ, Figure S21. IR stacked spectra N\_PSU, BMI.FO and N\_BMI.FO, Figure S22. IR stacked spectra N\_PSU, BMI.MAL and N\_BMI.MAL, Figure S23. IR stacked spectra N\_PSU, BMI.PRO and N\_BMI.PRO, Figure S24. D\_PSU membrane EDX, Figure S25. D\_BMI.PRO membrane EDX, Figure S26. D\_BMI.PIV membrane EDX, Figure S27. D\_BMI.BENZ membrane EDX, Figure S28. M\_5\_BMI.FO membrane EDX, Figure S29. D\_BMI.MAL membrane EDX, Figure S30. N\_PSU membrane EDX, Figure S31. N\_BMI.PRO membrane EDX, Figure S32. N\_BMI.PIV membrane EDX, Figure S33. N\_BMI.BENZ membrane EDX, Figure S34. N\_BMI.FO membrane EDX, Figure S35. N\_BMI.MAL membrane EDX, Figure S36. D\_Blank top surface CA with mili Q H<sub>2</sub>O, Figure S37. D\_Blank bottom surface CA with mili Q H<sub>2</sub>O, Figure S38. D\_Blank top surface CA with BMI.PRO, Figure S39. D\_Blank bottom surface CA with BMI.PRO, Figure S40. D\_Blank top surface CA with BMI.PIV, Figure S41. D\_Blank bottom surface CA with BMI.PIV, Figure S42. D\_Blank top surface CA with BMI.BENZ, Figure S43. D\_Blank bottom surface CA with BMI.BENZ, Figure S44. D\_Blank top surface CA with BMI.FO, Figure S45. D\_Blank bottom surface CA with BMI.FO, Figure S46. D\_Blank top surface CA with BMI.MAL, Figure S47. D\_Blank bottom surface CA with BMI.MAL, Figure S48. N\_Blank top surface CA with mili Q H<sub>2</sub>O, Figure S49. N\_Blank bottom surface CA with mili Q H<sub>2</sub>O, Figure S50. N\_Blank top surface CA with BMI.PRO, Figure S51. N\_Blank bottom surface CA with BMI.PRO, Figure S52. N\_Blank top surface CA with BMI.PIV, Figure S53. N\_Blank bottom surface CA with BMI.PIV, Figure S54. N\_Blank top surface CA with BMI.BENZ, Figure S55. N\_Blank bottom surface CA with BMI.BENZ, Figure S56. N\_Blank top surface CA with BMI.FO, Figure S57. N\_Blank bottom surface CA with BMI.FO, Figure S58. N\_Blank top surface CA with BMI.MAL, Figure S59. N\_Blank bottom surface CA with BMI.MAL, Table S1. D\_PSU weight percentage per element, Table 2. D\_BMI.PRO weight percentage per element, Table S3.

D\_BMI.PIV weight percentage per element, Table S4. D\_BMI.BENZ weight percentage per element, Table S5. D\_BMI.FO weight percentage per element, Table S6. D\_BMI.MAL weight percentage per element, Table S7. N\_PSU weight percentage per element, Table S8. N\_BMI.PRO weight percentage per element, Table S9. N\_BMI.PIV weight percentage per element, Table S10. N\_BMI.BENZ weight percentage per element, Table S11. N\_BMI.FO weight percentage per element, Table S12. N\_BMI.MAL weight percentage per element, Table S13. Ionic liquids density and 75% (*w/w*) solution density, Table S14. Ionic liquids 75% (*w/w*) solution viscosity, Table S15. Ionic liquids 75% (*w/w*) solution surface tension, Table S16. Solubilities for NMP membranes, Table S17. Solubilities for DMF membranes and Table S18. Solubility in pure ILs.

**Author Contributions:** Conceptualization, A.N.; methodology, D.D.H., A.G., R.G.-V. and A.N.; software, D.D.H.; validation, D.D.H., A.G. and A.N.; formal analysis, A.G. and A.N.; investigation, D.D.H., A.G. and A.N.; resources, A.G. and A.N.; data curation, D.D.H.; writing—original draft preparation, D.D.H. and A.N.; writing—review and editing, A.G., R.G.-V. and A.N.; visualization, D.D.H. and A.N.; supervision, A.N.; project administration, A.G., R.G.-V. and A.N.; funding acquisition, A.G. and A.N. All authors have read and agreed to the published version of the manuscript.

**Funding:** This research was funded by the European Union’s Horizon 2020 Research and Innovation Action program under the SunCoChem project, Grant Agreement No 862192.

**Institutional Review Board Statement:** Not applicable.

**Informed Consent Statement:** Not applicable.

**Data Availability Statement:** The data presented in this study are available on request from the corresponding author.

**Acknowledgments:** The authors would like to acknowledge the technical support of Scientific and Technical Resources Service of the URV, specifically for their help in the characterization of the membranes and ILs.

**Conflicts of Interest:** The authors declare no conflict of interest.

## References

1. Kazemifar, F.A. Review of Technologies for Carbon Capture, Sequestration, and Utilization: Cost, Capacity, and Technology Readiness. *Greenh. Gases Sci. Technol.* **2022**, *12*, 200–230. [[CrossRef](#)]
2. Modak, A.; Bhanja, P.; Dutta, S.; Chowdhury, B.; Bhaumik, A. Catalytic Reduction of CO<sub>2</sub> into Fuels and Fine Chemicals. *Green Chem.* **2020**, *22*, 4002–4033. [[CrossRef](#)]
3. World Resources Institute. *Climate Analysis Indicators Tool (CAIT)*; World Resources Institute: Washington, DC, USA, 2019.
4. Ghosh, S.; Modak, A.; Samanta, A.; Kole, K.; Jana, S. Recent Progress in Materials Development for CO<sub>2</sub> conversion: Issues and Challenges. *Mater. Adv.* **2021**, *2*, 3161–3187. [[CrossRef](#)]
5. Zhao, S.; Feron, P.H.M.; Deng, L.; Favre, E.; Chabanon, E.; Yan, S.; Hou, J.; Chen, V.; Qi, H. Status and Progress of Membrane Contactors in Post-Combustion Carbon Capture: A State-of-the-Art Review of New Developments. *J. Membr. Sci.* **2016**, *511*, 180–206. [[CrossRef](#)]
6. Blauwhoff, P.M.M.; Versteeg, G.F.; van Swaaij, W.P.M. A Study on the Reaction between CO<sub>2</sub> and Alkanolamines in Aqueous Solutions. *Chem. Eng. Sci.* **1983**, *38*, 1411–1429. [[CrossRef](#)]
7. Mota-Lima, A.; Alcantara, M.L.; Pérez-Sanz, F.J.; Bazito, R.C.; Vidinha, P.; Alves, R.M.B.; Nascimento, C.A.O. Review—High-Pressure Carbon Dioxide Separation Using Ionic Liquids: A CO<sub>2</sub>—Electrocatalysis Perspective. *J. Electrochem. Soc.* **2021**, *168*, 086502. [[CrossRef](#)]
8. Wasserscheid, P.; Keim, W. Ionic Liquids—New “Solutions” for Transition Metal Catalysis. *Angew. Chem. Int. Ed.* **2000**, *39*, 3772–3789. [[CrossRef](#)]
9. Dai, L.; Yu, S.; Shan, Y.; He, M. Novel Room Temperature Inorganic Ionic Liquids. *Eur. J. Inorg. Chem.* **2004**, *2004*, 237–241. [[CrossRef](#)]
10. Shobukawa, H.; Tokuda, H.; Susan, M.A.B.H.; Watanabe, M. Ion Transport Properties of Lithium Ionic Liquids and Their Ion Gels. *Electrochim. Acta* **2005**, *50*, 3872–3877. [[CrossRef](#)]
11. Simon, N.M.; Zanatta, M.; Neumann, J.; Girard, A.L.; Marin, G.; Stassen, H.; Dupont, J. Cation–Anion–CO<sub>2</sub> Interactions in Imidazolium-Based Ionic Liquid Sorbents. *ChemPhysChem* **2018**, *19*, 2879–2884. [[CrossRef](#)]
12. De los Ríos, A.P.; Irabien, A.; Hollmann, F.; Fernández, F.J.H. Ionic Liquids: Green Solvents for Chemical Processing. *J. Chem.* **2013**, *2013*, 2–4. [[CrossRef](#)]
13. Lei, Z.; Chen, B.; Koo, Y.M.; Macfarlane, D.R. Introduction: Ionic Liquids. *Chem. Rev.* **2017**, *117*, 6633–6635. [[CrossRef](#)] [[PubMed](#)]
14. Campisciano, V.; Giacalone, F.; Gruttadauria, M. *Supported Ionic Liquids: A Versatile and Useful Class of Materials*; The Chemical Record; John Wiley and Sons Inc.: New York, NY, USA, 2017; pp. 918–938. [[CrossRef](#)]

15. Wang, H.H.; Jung, J.T.; Kim, J.F.; Kim, S.; Drioli, E.; Lee, Y.M. A Novel Green Solvent Alternative for Polymeric Membrane Preparation via Nonsolvent-Induced Phase Separation (NIPS). *J. Membr. Sci.* **2019**, *574*, 44–54. [[CrossRef](#)]
16. Torras, C.; Garcia-Valls, R. Quantification of Membrane Morphology by Interpretation of Scanning Electron Microscopy Images. *J. Membr. Sci.* **2004**, *233*, 119–127. [[CrossRef](#)]
17. Nogalska, A. Ambient Carbon Dioxide Capture and Conversion via Membranes. Ph.D. Dissertation, Universitat Rovira i Virgili, Tarragona, Spain, 2018.
18. Nogalska, A.; Zukowska, A.; Garcia-Valls, R. Atmospheric CO<sub>2</sub> Capture for the Artificial Photosynthetic System. *Sci. Total Environ.* **2018**, *621*, 186–192. [[CrossRef](#)] [[PubMed](#)]
19. Tylkowski, B.; Carosio, F.; Castañeda, J.; Alongi, J.; García-Valls, R.; Malucelli, G.; Giamberini, M. Permeation Behavior of Polysulfone Membranes Modified by Fully Organic Layer-by-Layer Assemblies. *Ind. Eng. Chem. Res.* **2013**, *52*, 16406–16413. [[CrossRef](#)]
20. Gomez-Coma, L.; Garea, A.; Irabien, A. Carbon Dioxide Capture by [Emim][Ac] Ionic Liquid in a Polysulfone Hollow Fiber Membrane Contactor. *Int. J. Greenh. Gas Control* **2016**, *52*, 401–409. [[CrossRef](#)]
21. Ramos, V.C.; Han, W.; Zhang, X.; Zhang, S.; Yeung, K.L. Supported Ionic Liquids for Air Purification. *Curr. Opin. Green Sustain. Chem.* **2020**, *25*, 100391. [[CrossRef](#)]
22. Patil, T.; Dharaskar, S.; Sinha, M.; Jampa, S.S. Effectiveness of Ionic Liquid-Supported Membranes for Carbon Dioxide Capture: A Review. *Environ. Sci. Pollut. Res.* **2022**, *29*, 35723–35745. [[CrossRef](#)]
23. Dupont, J.; Consorti, C.S.; Suarez, P.A.Z.; Souza, R.F. Preparation of 1-Butyl-3-Methyl Imidazolium-Based Room Temperature Ionic Liquids. *Org. Synth.* **2003**, *79*, 236. [[CrossRef](#)]
24. Horcas, I.; Fernández, R.; Gómez-Rodríguez, J.M.; Colchero, J.; Gómez-Herrero, J.; Baro, A.M. WSXM: A Software for Scanning Probe Microscopy and a Tool for Nanotechnology. *Rev. Sci. Instrum.* **2007**, *78*, 013705. [[CrossRef](#)] [[PubMed](#)]